

On the physisorption of water on graphene: Sub-chemical accuracy from many-body electronic structure methods

Jan Gerit Brandenburg,^{†,‡,@} Andrea Zen,^{†,‡,@} Martin Fitzner,^{†,‡} Benjamin
Ramberger,[¶] Georg Kresse,[¶] Theodoros Tsatsoulis,^{§,||} Andreas Grüneis,^{§,||}
Angelos Michaelides,^{*,†,‡} and Dario Alfe^{*,⊥,‡,#}

[†]*Department of Physics and Astronomy, University College London, Gower Street, London
WC1E 6BT, United Kingdom*

[‡]*Thomas Young Centre and London Centre for Nanotechnology, 17-19 Gordon Street,
London WC1H 0AH, United Kingdom*

[¶]*University of Vienna, Faculty of Physics and Center for Computational Materials
Sciences, Sensengasse 8/12, 1090 Wien, Austria*

[§]*Institute for Theoretical Physics, Vienna University of Technology, Wiedner Hauptstrasse
8-10, 1040 Vienna, Austria*

^{||}*Max Planck Institute for Solid State Research, Heisenbergstrasse 1, 70569 Stuttgart,
Germany*

[⊥]*Department of Earth Sciences, University College London, Gower Street, London WC1E
6BT, United Kingdom*

[#]*Dipartimento di Fisica Ettore Pancini, Università di Napoli Federico II, Monte S.
Angelo, I-80126 Napoli, Italy*

[@]*These two authors contributed equally*

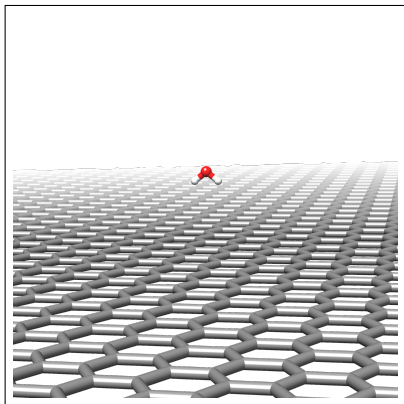
E-mail: angelos.michaelides@ucl.ac.uk; d.alfe@ucl.ac.uk

Abstract

Wet carbon interfaces are ubiquitous in the natural world and exhibit anomalous properties, which could be exploited by emerging technologies. However, progress is limited by lack of understanding at the molecular level. Remarkably, even for the most fundamental system (a single water molecule interacting with graphene), there is no consensus on the nature of the interaction. We tackle this by performing an extensive set of complementary state-of-the-art computer simulations on some of the world's largest supercomputers. From this effort a consensus on the water-graphene interaction strength has been obtained. Our results have significant impact for the physical under-

standing, they indicate that the interaction is weaker than predicted previously. They also pave the way for more accurate and reliable studies of liquid water at carbon interfaces.

Graphical TOC Entry



Introduction

The adsorption and diffusion of molecules on surfaces is central to countless industrial applications, including catalysis, gas storage, desalination, and more. Of all the many and varied molecular adsorption systems, few, if any, are of greater importance than those involving water and carbon. Such interfaces are, for example, at the very heart of water purification and desalination membranes. In addition, water-carbon interfaces are incredibly interesting scientifically in that they can exhibit unique and fascinating behavior.¹⁻⁹ For example, water can flow in an essentially frictionless manner across the surfaces of sp^2 -bonded carbon materials (both carbon nanotubes and graphene).^{6,10-12} However, seemingly similar materials such as nanotubes made from hexagonal boron nitride do not exhibit such behaviour.^{6,7,13-15} Apart

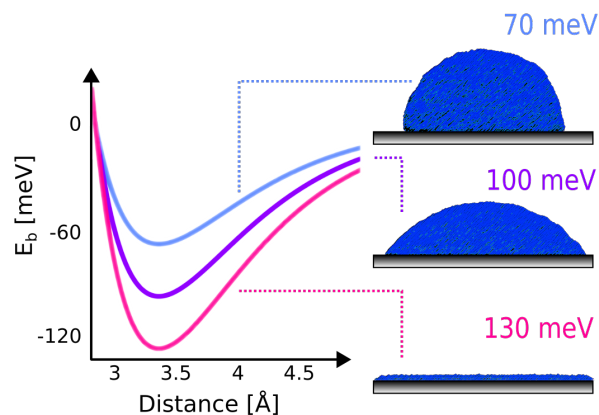


Figure 1: Water droplet modeled by a coarse-grained water model (mW) and Morse-type water-wall potential with varying adsorption strengths (see Fig. 6). This figure illustrates that modest changes in the adsorption energy lead to drastic changes in the wetting properties of the surface.

from water purification, wetting of surfaces is of general interest and graphene can be seen as representative van der Waals (vdW) material. Many of these exciting experiments showing exceptional properties of water on graphitic surfaces and the outstanding applications lack a full molecular level understanding of the processes and the mechanisms involved. In order to gain further insight, it is necessary to com-

plement experimental investigations with theoretical approaches. The most fundamental property of any adsorption system is the question of the adsorption bond itself, what the strength of the interaction is, the orientation of the molecule, and the physical nature of the interaction. For water-carbon interfaces at their simplest level, this comes down to understanding how a single water molecule bonds to a single sheet of graphene. Accurately establishing the strength of this interaction is important because it directly impacts upon the behavior of water at graphitic surfaces. For instance, as illustrated in Fig. 1, molecular dynamics simulations (see also Fig. 6) reveal that altering the strength of the water-graphene interaction by as little as 60 meV transforms the graphene surface from hydrophobic to hydrophilic. The hydrophobicity of water on graphene has been subject of intensive debate. Approaches targeting the contact angle theoretically^{16–18} as well as experimentally^{19,20} yield controversial conclusions. A recent experimental estimate that does not rely on a support lattice gives a water contact angle of $42\pm 3^\circ$,²⁰ while the results from computer simulations spread from 0° to 90° due to the sensitivity to the water-carbon interaction parameter. Accurate estimates of this interaction will help to solve this hydrophobicity conundrum.

Experimentally, water molecules readily form clusters on surfaces and graphene is no exception.²¹ This has so far prohibited single molecule adsorption measurements of water on graphene. On the other hand, the subtle balance of the contributing intermolecular interactions and the very high accuracy required makes the theoretical description by electronic structure methods challenging. Indeed, adsorption energy estimates have to be more accurate than so called “chemical accuracy”, which is defined as 1 kcal/mol or 43 meV, in order to be useful in this system. This is often beyond the accuracy delivered by density functional theory (DFT); the most widely used electronic structure method for understanding molecules at surfaces. Indeed, previous work has shown that DFT can provide any value for the water adsorption strength on graphene between 0 and -

160 meV depending on the exchange-correlation functional and vdW-correction.^{22–27}

Table 1: Equilibrium adsorption energies E_{ad} of a single water monomer on graphene as estimated from various electronic structure methods.

$E_{\text{ad}}/\text{meV}^a$	Method	Comment
-130	DFT/CC	Corrects DFT based on differences on small cluster ²⁸
-130	DFT-SAPT	Extrapolation from cluster ²⁹
-70 ± 10^c	DMC	Periodic system, large stochastic error, finite-size effects ²²
-135	i-CCSD(T)	Incremental expansion, correlation from cluster, small basis set ³⁰
-87	p-CCSD(T)	Periodic system, finite-size corrected ^b
-99 ± 6^c	DMC	Periodic system, finite-size corrected ^b

^aWater in the so-called “2-leg” configuration; see Fig.

2 ^bThis work. ^cError due to DMC stochastic uncertainty.

The variation in adsorption energies obtained from DFT calls for many-body methodologies that can be rigorously converged. The application of such methods to extended (periodic) surfaces, however, does not come without significant challenges.³¹ Table 1 summarizes attempts to provide benchmark quality binding energies for water on graphene with state-of-the-art electronic structure methods.^{22,28–30,32} It can be seen that the previous estimates range from about 70 to about 130 meV. Whilst this is narrower than the range obtained from DFT, the deviations are clearly too high to make faithful predictions on the water-graphene interactions. Although these previous attempts have involved great care and considerable effort, they all have possible weaknesses and potential shortcomings. Here, in light of a new estimate of the adsorption energy of water on graphene, we will critically examine previous estimates and in so-doing resolve the discrepancies between previous reports. Our new study relies on impressive progress with state-of-the-

art electronic structure methods and their implementation in scalable software suits in the past few years. These developments together with an increased capacity of available computational resources makes the accurate determination of binding energies on extended surfaces feasible. It is thus timely to analyze the physisorption of water on graphene again and in so-doing we are able to demonstrate that different many-body electronic structure methods indeed agree within sub-chemical accuracy.

Quantum-mechanics based computer simulations

Various computational approaches have been used in the current study. Here, mainly for orientation purposes, we briefly comment on the structures examined, the quantities computed, and the main methods used. Full details of all methods are provided in *Computational Details* section.

Water monomer adsorption was considered in three different motifs, dubbed 0-leg, 1-leg, and 2-leg as defined in Fig. 2. These are the most widely discussed adsorption structures in previous studies.^{22,28–30,32} The adsorption energy E_{ad} is the minimum, obtained at the equilibrium distance d_{ads} , of the binding curve:

$$E_{\text{b}}(d) = E_{\text{W+G}}(d) - E_{\text{W+G}}(d_{\text{far}}), \quad (1)$$

where $E_{\text{W+G}}(d)$ is the energy of the system with the water at a distance d from the graphene sheet, and $E_{\text{W+G}}(d_{\text{far}})$ is the energy of the non-interaction system, with water far away at a distance d_{far} from graphene.³³ Note that what is computed here is the static electronic energy without inclusion of thermal or nuclear quantum effects.

One of the key techniques used in this study is diffusion Monte-Carlo (DMC).³⁴ DMC can be readily applied to periodic systems and in the past few years the computational efficiency and accuracy of the technique has improved significantly. In particular, a recent algorithmic development has reduced computational effort by up to two orders of magnitude.³⁵ Subsequently it was shown that the new DMC algorithm to-

gether with an effective estimation of finite-size errors yields chemically accurate lattice energies for a range of molecular crystals (including ice and delocalized π -systems) with modest computational cost.³⁶ In the current study we performed DMC studies with the CASINO code³⁷ for water on benzene, coronene, and graphene in periodic unit cells. For adsorption on graphene a large 5×5 unit cell was employed.

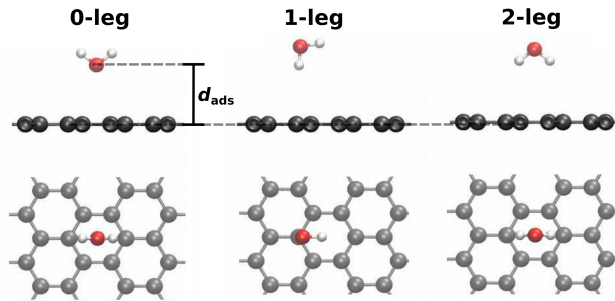


Figure 2: Water adsorption structures considered. We show the 0-leg, 1-leg, and 2-leg motif each from the side (top) and from above (bottom). The distance d is defined by the distance of the oxygen atom from the graphene plane. A periodic 5×5 graphene cell is used in most calculations, while for clarity only a small part of the simulation cell is shown. All equilibrium geometries are provided, see *Supporting Information*.

The second many-body approach used in this study is coupled cluster, for both water adsorption on benzene and coronene and on periodic graphene. Specifically, we used linear scaling domain based pair natural orbital coupled cluster including singles, doubles, and perturbative triples [denoted here as the L-CCSD(T) method³⁸], as implemented in the ORCA program package³⁹ for the finite sized cluster models. Periodic coupled cluster including singles, doubles, and perturbative triples [denoted here as the p-CCSD(T)] was used for adsorption on graphene.⁴⁰ For these calculations a periodic 4×4 unit cell was employed and the coupled cluster code CC4S interfaced to the VASP code^{41,42} was used.^{43,44}

The third many-body approach employed is the random phase approximation (RPA),^{45–49} which computes the correlation energy based on the electron density response function. RPA is computationally more affordable than

CCSD(T) and has recently shown good results, in particular if singles corrections are introduced.^{36,50–52} However, it includes fewer excitation types than CCSD(T) and thus one has to carefully test its accuracy. Here we used RPA based on PBE orbitals, i.e. the exact exchange energy EXX@PBE combined with the correlation RPA@PBE. In addition, the contribution from GW single excitations (GWSEs) was computed based on the work of Klimeš et al.⁵³

Note that the calculations with the various methods used the same adsorption structures (generated from DFT optimizations), and as reference the isolated fragments with fixed (unrelaxed) geometries are taken.

Results

High-level adsorption energies

Interaction energy curves of water adsorbed in three different configurations (0-leg, 1-leg, 2-leg, see Fig. 2) on benzene, coronene, and graphene have been computed with a range of many-body methods. Here, DMC as well as CCSD(T) are considered benchmark quality methods, while RPA is tested as a cheaper alternative. Due to the smaller unit cell used in p-CCSD(T), we expect that DMC provides the best reference interaction energies for water adsorbed on graphene. Combined interaction energy curves for the considered systems are shown in Fig 3, and interpolated minima are given in Table 2.

We begin by noting that the 0-leg configuration on benzene is purely repulsive (i.e. unbound), while it gets increasingly attractive on coronene and graphene. This trend is consistent with all methodologies and DMC and L-CCSD(T) agree within 2 meV for this binding motif. In contrast, both the 1-leg and 2-leg structures bind on benzene, with the 2-leg adsorption 5-11 meV stronger. This binding energy difference increases on coronene to 15-22 meV. This is due to a decreased binding energy of the 1-leg motif (from benzene to coronene), while the 2-leg binding is identical from DMC and RPA and even slightly stronger from L-CCSD(T). In stark contrast to the be-

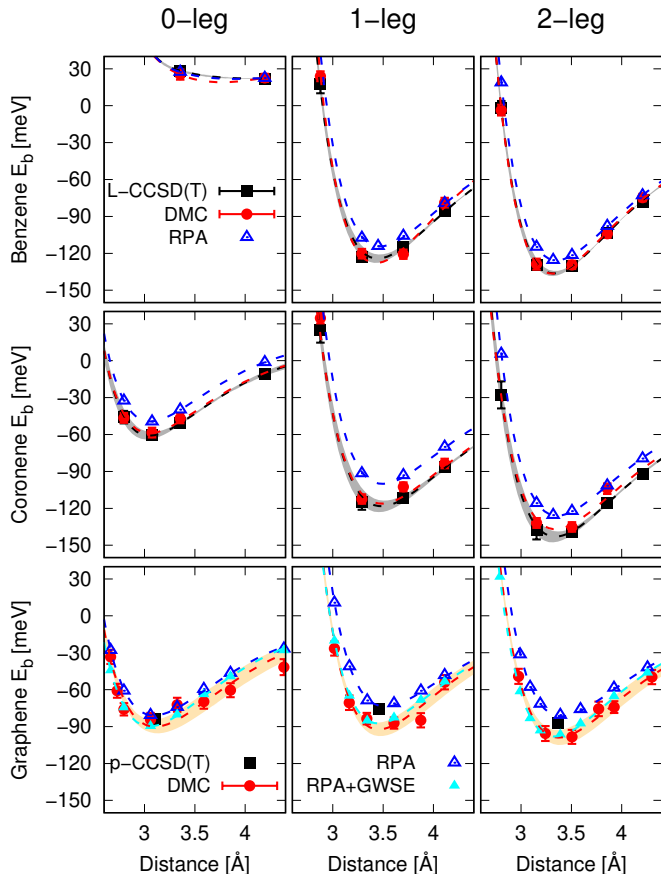


Figure 3: Binding energy curves of water on benzene (top), coronene (middle), and graphene (bottom) in the 0-leg, 1-leg, and 2-leg motifs computed with the many-body electronic structure methods L-CCSD(T), DMC, and RPA. Error bars in DMC correspond to the stochastic error (1 standard deviation), in L-CCSD(T) to the basis set uncertainty. Dashed lines are fits via a Morse potential (see *Supporting Information*).

havior observed on the small molecules, on periodic graphene the 0-leg, 1-leg, and 2-leg structures have very similar DMC binding energies of -90 ± 6 , -92 ± 6 , and -99 ± 6 meV, respectively. Interestingly, this includes the 0-leg configuration which on benzene was purely repulsive. The contrast between benzene and graphene for the 0-leg motif is quite remarkable and will be commented on in more detail later.

The benchmark quality methods DMC and L-CCSD(T) agree with each other on the molecular clusters with a maximum error of 12 meV on the single point evaluations and 6 meV for the interpolated binding energies. Similarly, the DMC and CCSD(T) equilibrium binding en-

Table 2: Equilibrium binding distances d_{ad} and energies E_{ad} of single water monomer on benzene, coronene, and graphene from DMC, L-CCSD(T), p-CCSD(T), RPA, and RPA+GWSE. Distances are given in Å and energies in meV.

	DMC ^a		L-CCSD(T) ^a		RPA ^a			
	$d_{\text{ad}}/\text{Å}$	E_{ad}/meV	$d_{\text{ad}}/\text{Å}$	E_{ad}/meV	$d_{\text{ad}}/\text{Å}$	E_{ad}/meV		
benzene								
0-leg	not binding		not binding		not binding			
1-leg	3.43(2)	-128(5)	3.45(2)	-124(3)	3.47(1)	-114(3)		
2-leg	3.31(1)	-136(5)	3.32(1)	-136(2)	3.35(1)	-126(1)		
coronene								
0-leg	— ^b	-59(5)	3.05(3)	-61(3)	3.06(1)	-49(2)		
1-leg	— ^b	-116(4)	3.48(3)	-118(5)	3.49(1)	-100(4)		
2-leg	— ^b	-137(4)	3.34(3)	-143(4)	3.36(1)	-126(2)		
	DMC ^a		p-CCSD(T)		RPA ^a		RPA+GWSE ^a	
	$d_{\text{ad}}/\text{Å}$	E_{ad}/meV	$d_{\text{ad}}/\text{Å}$	E_{ad}/meV	$d_{\text{ad}}/\text{Å}$	E_{ad}/meV	$d_{\text{ad}}/\text{Å}$	E_{ad}/meV
graphene								
0-leg	3.10(3)	-90(6)	— ^c	-84	3.09(1)	-81(2)	3.05(1)	-90(2)
1-leg	3.46(3)	-92(6)	— ^c	-76	3.52(1)	-74(1)	3.45(1)	-87(1)
2-leg	3.37(2)	-99(6)	— ^c	-87	3.41(1)	-82(1)	3.33(1)	-98(1)

^aPotentials curves (see Fig. 3) are interpolated with a Morse potential, yielding E_{ad} , d_{ad} , and the corresponding errors that is a combined stochastic and fitting error for DMC (reported in parenthesis relative to the last significant digit, see *Supporting Information*). ^bDMC value for d_{ad} is not estimated, as the calculated DMC points for water on coronene are not enough for a four parameter fit. We assume that d_{ad} is the same as L-CCSD(T) and we estimate only E_{ad} . ^cp-CCSD(T) value calculated only in a single point, at d_{ad} 3.10 Å for the 0-leg, 3.46 Å for the 1-leg, 3.37 Å for the 2-leg.

energies on graphene have only small deviations between 6 and 16 meV. As the two electronic structure methods have quite distinct foundations, this gives us confidence in the high accuracy of the reported binding energies. RPA consistently underbinds all structures by about 9-18 meV, this underestimation is effectively reduced by the singles corrections. The GW based density corrections also change the relative binding of the three motifs, making the 2-leg 8 meV more stable than the 0-leg (in agreement with DMC and CCSD(T)). The observed trend of underestimated RPA binding energies and highly accurate RPA+GWSE energies is consistent with previous findings on molecular adsorption⁵⁴ and molecular crystal lattice energies.⁵² From the interpolated potential energy curves, we additionally extract the equilibrium adsorption distance and energy (see Table 2). The distances from all many-body methods are in good agreement with each other with a maximum difference of 0.06 Å. Our best DMC estimate for the water adsorption

energy on graphene in the lowest energy 2-leg configuration (-99 ± 6 meV) is in between previously reported binding energies. The p-CCSD(T) adsorption energy is in very good agreement, though the binding is at -87 meV slightly lower. This might be due to finite-size or coverage effects (originating from the smaller 4×4 cell employed) and some remaining sensitivity to the basis set. We note that the remaining finite coverage effects have only been corrected for on the level of Hartree-Fock (HF) theory.

Comparison to literature values

As the revised binding energy differs from previously reported values (see Table 1), we carefully investigated the previously used numerical settings and assumptions. First, the difference with the earlier DMC value of -70 ± 10 meV,²² can be explained by the larger statistical errors (smaller precision) and remaining finite-size effects of the older study. On both points, the present study has been improved substantially.

The incremental CCSD(T) based adsorption energies are 30 to 35 meV more strongly bound than the DMC values reported here.³⁰ The higher uncertainty of the previous study compared to the DMC and p-CCSD(T) values of this work can be attributed to the orbital basis set employed in the earlier study. Specifically, a mixed double- ζ /triple- ζ basis set expansion was used and as shown in Fig. 7 for the water-benzene interaction this does not yield fully converged adsorption energies. Although these basis set tests have been performed with benzene as the substrate and some basis set errors at the HF and correlation level partially cancel, the extent of error cancellation cannot be predicted and we expect a significantly increased accuracy from our p-CCSD(T) calculations.

The other studies listed in Table 1 use finite-sized clusters to approach the periodic system. Given the variation in adsorption energies and different nature of the adsorption bond (see Fig. 5) upon going from benzene, to coronene, to graphene any estimate of the adsorption energy on graphene based on extrapolations from clusters must be done with extreme care. Whilst slightly different from ear-

lier studies,^{28,29} we illustrate the challenge in Fig. 4 where the adsorption energy of the three binding motifs is plotted as a function of cluster size.⁵⁵ In particular, from Fig. 4 it can be seen that whilst there is a monotonic convergence towards the adsorption energy on graphene for all adsorption motifs, the extrapolation using benzene and coronene data gives a reasonable result only for the 1-leg structure. The extrapolation for both the 0-leg and 2-leg geometries substantially overestimates the adsorption energy and we see a remarkable sensitivity towards the water orientation. Although not reported in the figure this trend is even slightly stronger using the L-CCSD(T) data, where the 2-leg adsorption energy increases from benzene to coronene, i.e. a qualitatively different convergence trend towards graphene.⁵⁶ The pronounced contrast in the adsorption energies of the different motifs on small substrates compared to graphene is quite striking. Overall this suggests for such a delicate system as water on graphene adsorption energies obtained directly on periodic models are likely to be more reliable than those obtained with cluster models.

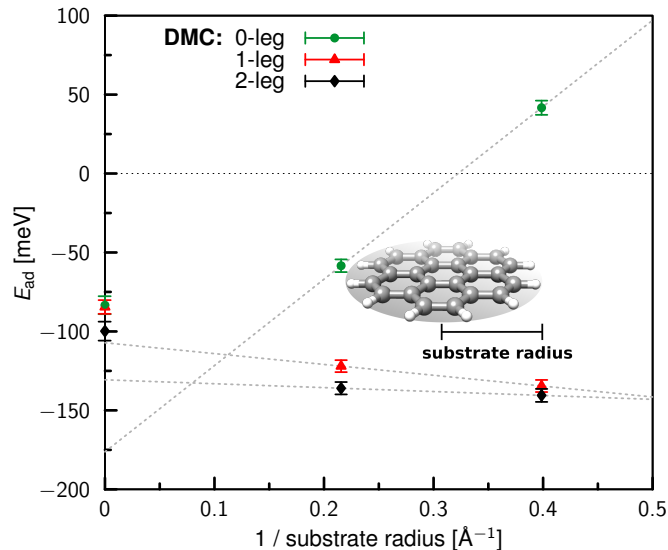


Figure 4: Water adsorption energies at fixed equilibrium distances on graphene, coronene, and benzene plotted as a function of (inverse) substrate size. Following the size definition used in Ref.⁵⁵ benzene is 0.40 \AA^{-1} , coronene is 0.22 \AA^{-1} , and graphene is 0 \AA^{-1} . Dashed lines are fitted using benzene and coronene data.

Implications of revised adsorption energies

Large scale dynamics studies of water at graphitic interfaces have been performed in the past years using classical water force fields combined with Lennard-Jones parameters for the oxygen-carbon interaction.^{7,10,12,16,57-59} Parameters have been adjusted to reference data from quantum chemistry on graphene-like clusters⁶⁰ or by reproducing experimental data like the contact angle of a water droplet on graphite.^{61,62} Our study has two major implications apart from an increased scepticism regarding the older theoretical reference data. First, we find that a Morse potential is much better suited to describe the water molecule-graphene interaction compared to Lennard-Jones potentials (Fig. 3 and *Supporting Information*). Furthermore, a coarse-grained model describing the interaction only as a carbon-oxygen interaction cannot describe both the 0-leg and 2-leg adsorption motifs simultaneously, i.e. the

hydrogen-carbon interactions are mandatory for a qualitatively correct description. Still, we can use our revised adsorption energy curves to estimate the contact angle of a water droplet on graphene in a coarse-grained manner using a wall potential for graphene instead its atomistic structure. Our dynamics simulations indicate a contact angle of 56° (see Fig. 6). We expect this to be an upper bound as the presence of other water molecules should screen the effective monomer adsorption strength. This is consistent with a recent experimental estimate of $42 \pm 3^\circ$,²⁰ both pointing to a mild hydrophilicity of graphene. Additional experiments could in principle establish the line tension of water on graphene, which would be a potential test of our theoretical results. In order to correctly predict the line tension, the water-graphene potential used in computational studies needs not only reproduce the strength but also the whole interaction curve (see Fig. 6). Our new data will be valuable for further DFT and potential refinements, though for faithful predictions additional non-equilibrium geometries and high water coverages are needed.

Analyzing the nature of the water-graphene interaction

We now briefly discuss the nature of the interaction between water and graphene. As part of our analysis we examined how, at the DFT level, the electronic charge density rearranges upon creation of the adsorption bond. This is shown in Fig. 5 for the three binding motifs. Charge density rearrangement plots such as this provide a pictorial representation of how the electron density rearranges upon adsorption. The key features revealed by Fig. 5 are that: (i) The most extensive areas of charge rearrangement are on the water molecule and in the immediate vicinity of each adsorption site; (ii) The extent of the charge density rearrangement is fairly long ranged; carbon atoms as far as 8 Å from the molecule exhibit some (albeit small) change in their charge density; and (iii) In all configurations the electronegative oxygen atom gains charge density, while the hydrogens lose charge density. The key difference

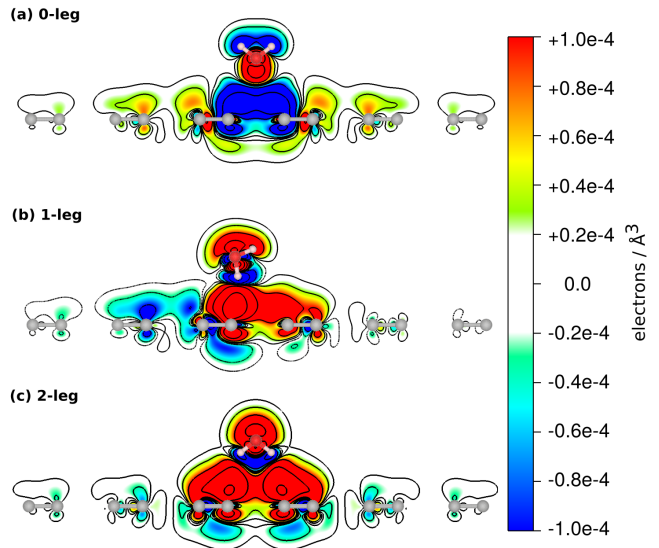


Figure 5: Electronic density change upon binding water on graphene in the equilibrium geometry for the (a) 0-leg, (b) 1-leg, and (c) 2-leg configurations. Planes perpendicular to the surface that bisect the water molecules are shown. Red regions indicate density increase upon binding; blue regions indicate depletion. Electronic density was calculated with DFT, using the PBE functional in a 5×5 unit cell.

between the 0-leg motif and the others is that in the 0-leg structure the negative oxygen ion points towards the graphene layer, and induces a charge loss in the local area surrounding it. Part of the charge is transferred to the water molecule, while the rest is redistributed within the graphene layer. This charge rearrangement in the substrate is slightly more extensive in the 0-leg structure than in the two other binding motifs, which explains in part the strong variation of the 0-leg adsorption energy upon going from benzene to graphene. Note that the qualitatively different nature of the adsorption bond for the 0-leg motif compared to the others has an impact on the surface dipole moment and thus the work function of the substrate. Indeed at the water coverage considered, the DFT PBE based work functions are 3.7, 4.5, and 4.8 meV for the 0-leg, 1-leg and 2-leg motifs, respectively. The differences are quite pronounced and could in principle be observable experimentally. In addition, as the molecule rotates on or diffuses across the surface the nature

of the charge rearrangement is likely to vary rapidly and so too the work function.

A more quantitative analysis of the adsorption bond has been performed with symmetry adapted perturbation theory for the small substrate models (SAPT⁶³⁻⁶⁶). The results of this analysis are reported in *Supporting Information*. The key conclusion from this analysis is that the electrostatic component to the interaction is attractive for the 1-leg and 2-leg motifs, while it is repulsive for the 0-leg motif on benzene. However, this repulsive interaction decreases significantly for larger substrate sizes and at the same time the attraction from vdW interactions increases. We can overall conclude from this analysis that the 1-leg and 2-leg motifs behave in a rather similar manner, while the 0-leg motif has a quite distinct electrostatic interaction along with a more pronounced charge reorganization in the substrate.

Conclusions

To conclude, we have computed the adsorption of a water monomer on a periodic graphene sheet with DMC, CCSD(T), and RPA. By comparison to RPA and to L-CCSD(T) on smaller aromatic substrates, we have been able to resolve discrepancies between previously published adsorption energies. We have shown that different water orientations have quite distinct interactions with the graphene layer, but that ultimately they yield very similar binding energies. Cheaper computational methods such as DFT have shown that the potential energy surface for water on graphene is very smooth. However, here we show for the first time from accurate many-body electronic structure methods that there is almost no orientational dependence in the water monomer adsorption energy. Whilst more work is needed, this could have implications for and could partly explain the very low friction coefficient of liquid water on sp²-bonded carbon. We hope that the benchmark provided here will be of value in larger scale *ab initio* MD and classical MD studies of water on graphene and other sp²-bonded carbon materials. Together with previous studies using a range of many-body methods to study ad-

sorption on hexagonal boron-nitride (hBN),⁵⁴ carbon nanotubes,⁶⁷ clays,⁶⁸ and lithium hydride,^{69,70} our study demonstrates that adsorption energies on extended surfaces can now be computed with sub-chemical accuracy. These electronic structure approaches are becoming a robust and reliable tool and have the prospect of been applied routinely to surface adsorption problems.

Acknowledgement We are grateful for discussions with Francesco Paesani and Narbe Mardirossian. J.G.B acknowledges support by the Alexander von Humboldt foundation within the Feodor-Lynen program. A.Z. and A.M. are supported by the European Research Council (ERC) under the European Unions Seventh Framework Program (FP/2007-2013)/ERC Grant Agreement 616121 (HeteroIce project). A.Z. and A.M.s work was also sponsored by the Air Force Office of Scientific Research, Air Force Material Command, US Air Force, under Grant FA8655-12-1-2099. We are also grateful, for computational resources, to ARCHER UK National Supercomputing Service, United Kingdom CarParrinello (UKCP) consortium (EP/F036884/1), the London Centre for Nanotechnology, University College London (UCL) Research Computing, Oak Ridge Leadership Computing Facility (DE-AC05-00OR22725), and IT4Innovations Center of Excellence (CZ.1.05/1.1.00/02.0070 and LM2015070), and the UK Materials and Molecular Modelling Hub, which is partially funded by EPSRC (EP/P020194/1). A.G. and T.T. acknowledge funding from the European Research Council (ERC) under the European Unions Horizon 2020 research and innovation program (grant agreement No 715594). p-CCSD(T) calculations were conducted on the HPC system COBRA of the Max Planck Computing and Data Facility (MPCDF).

Supporting Information Available

The following files are available free of charge.

- supinfo.pdf: Provides details on the

setup for the DMC and L-CCSD(T) calculations, individual interaction energies from many-body methods, fit with Morse potential, work function from DFT, and energy partitioning from symmetry adapted perturbation theory. Geometries of considered water configurations and parameters of reference Morse potentials for benchmark purposes are given.

- water-graphene-morse.xlsx: Parameters of reference Morse potentials.
- water-graphene-geoms.zip: Geometries used for the adsorption energy calculation.

Computational Details

We consider water adsorption in three different motifs, dubbed 0-leg, 1-leg, and 2-leg as defined in Fig. 2. In order to be consistent with previous DMC calculations, the geometries are taken from PBE⁷¹ optimizations, yielding the bond lengths $R(\text{C-C}) = 1.423 \text{ \AA}$ within the graphene sheet, $R(\text{O-H}) = 0.972 \text{ \AA}$ for the hydrogen atom pointing towards the surface in the 1-leg motif and $R(\text{O-H}) = 0.97 \text{ \AA}$ otherwise. The hydrogen atoms of the water molecule have the usual bond angle of $\angle\text{HOH} = 104.4^\circ$. The adsorption distance d_{ad} is defined by the distance of oxygen to the graphene plane. Molecular clusters have been cut out of the periodic system and saturated with hydrogens. Here, we use fixed experimental bond lengths of $R(\text{C-C}) = 1.42 \text{ \AA}$, $R(\text{O-H}) = 0.957 \text{ \AA}$, and $R(\text{C-H}) = 1.089 \text{ \AA}$. Based on PBE-D3 calculations,⁷¹⁻⁷³ we have tested that the different bond lengths give rise to a binding energy difference below 1.5 meV.

Contact angle from molecular dynamics simulations

The simulations to demonstrate the influence of the adsorption energy on the contact angle were done using the coarse-grained mW model⁷⁴ of water and a Morse wall potential that acts as a function of the z coordinate. The distance parameter was fitted to reproduce the DMC interaction curve for the 2-leg conformation. The resulting interaction curves, together with Lennard-Jones 9-3 and 12-6 wall variants, can be seen in Fig. 6 (upper panel).

To obtain contact angles we performed computations with the LAMMPS⁷⁵ software, integrating the equations of motion with a timestep of 10 fs in the NVT ensemble utilizing a 10-fold Nosé-Hoover chain⁷⁶ with a relaxation time of 1 ps to realize a temperature of 300 K for a total time of 20 ns (an additional initial

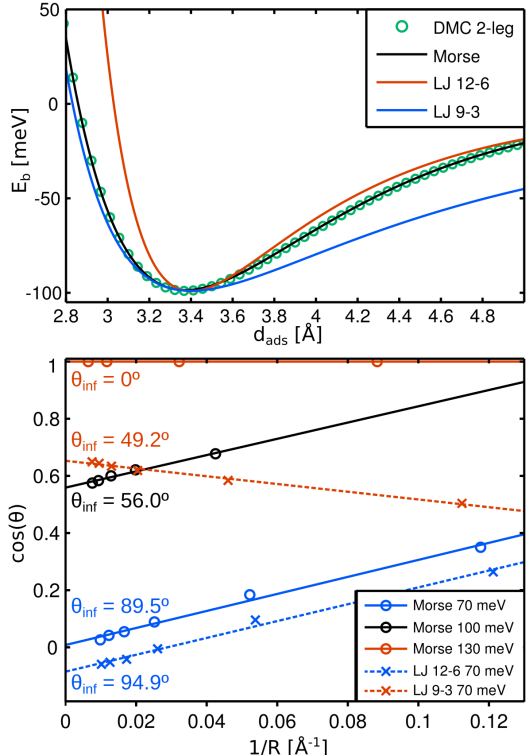


Figure 6: Water adsorption modeled by a coarse-grained water model (mW) and different wall potentials. The upper panel shows the water-wall interaction potentials for an interaction strength of 100 meV. The lower panel shows the results for contact angles of different sized droplets, from which we extract the contact angle θ_{inf} for an infinitely large droplet. The slope is related to the line tension of water on graphene (see eq. 2).

10 ns to relax the droplet shape were discarded). From the trajectories we obtained the radial density profile of the liquid and fitted this to a spherical cap shape which yields the contact angle (we did not find any significant deviations from spherical shape). We performed this calculation for droplet sizes ranging from ~ 600 to $\sim 70,000$ molecules, fitting the size-dependent contact angles to the line-tension modified Young’s equation:⁷⁷

$$\cos(\theta_R) = \cos(\theta_{\text{inf}}) - \frac{1}{\gamma_{\text{lv}}} \frac{\tau}{R} \quad (2)$$

which results in the contact angle for an infinitely large water droplet. Here, θ_R is the measured contact angle for a given droplet, θ_{inf} is the contact angle of the infinite droplet, γ_{lv} is the liquid vapor surface tension (which does not need to be known for a fit), τ is the line tension and R is the average radius of the contact area between the droplet and the wall. The results can be seen in Fig. 6 (lower panel) and show a stark influence of the contact angle to the used interaction strength and potential type. The simulation cells were periodic in x and y dimensions and with roughly $40 \text{ nm} \times 40 \text{ nm}$ large

enough to avoid self-interaction of the water molecules even for the complete wetting geometry in all cases but for the largest droplets.

Random phase approximation

We use RPA as implemented in Turbomole 7.2⁷⁸ for molecular complexes and a developer version of VASP 6^{41,42} for graphene. The CP corrected complexation energy of A and B in basis sets a and b are computed via

$$E_{CP}^{\text{int}} = E^{\text{int}} + E_{CP} \quad (3)$$

$$E^{\text{int}} = E(AB_{ab}) - E(A_a) - E(B_b) \quad (4)$$

$$E_{CP} = E(A_a) - E(A_{ab}) + E(B_b) - E(B_{ab}) \quad (5)$$

The Hartree and exact exchange energies (HXX@PBE) and the RPA correlation energy (RPA@PBE) are extrapolated to the basis set limit with optimized exponents.⁷⁹ The final interaction energy is given by the extrapolated CP corrected energies E_{CP}^{int} with a basis set error estimated as $|E_{CP}|/2$. For the periodic system, PAWs with energy cutoff of 430 eV are used. The results were extrapolated to the basis set limit assuming that errors drop off like one over the basis set size.^{46,80} A quadrature with 8 grid points was used for the evaluation of the imaginary time and frequency integrations.⁸¹ The adsorption curves have been computed with 14 Å vacuum corrected with an increased vacuum of 20 Å at the equilibrium geometry. Convergence of the first Brillouin zone sampling has been tested with additional calculations using $2 \times 2 \times 1$ k -points and a $4 \times 4 \times 1$ supercell (the two settings correspond to 25 and 64 points in the Brillouin zone of a primitive graphene cell).

Coupled cluster theory

We use the linear scaling domain based pair natural orbital CCSD(T) [denoted here as the LCCSD(T)] method³⁸ as implemented in the ORCA program package.³⁹ The implementation has been optimized to use compact representations of all amplitudes and imposing block sparsity of tensors.⁸² Non-augmented basis sets are used in the CCSD(T) calculations to ensure numerically stable convergence on larger substrates. Though convergence of correlation energies with the employed basis sets is well studied,^{83–86} it is mandatory to carefully test convergence for our target system and numerical settings. In Fig. 7, we show the convergence of uncorrected and CP-corrected Hartree-Fock (HF) and correlation E_{corr} binding energies. As usual for self-consistent field solutions, the plain HF interaction energies overestimate the binding due to basis set superposition error (BSSE). The BSSE is quite effectively removed by the CP correction and for basis sets of about TZ quality can yield reasonably accurate results. Still, the HF calculation is not the bottleneck in our study and we thus use direct extrapolations with QZ and 5Z

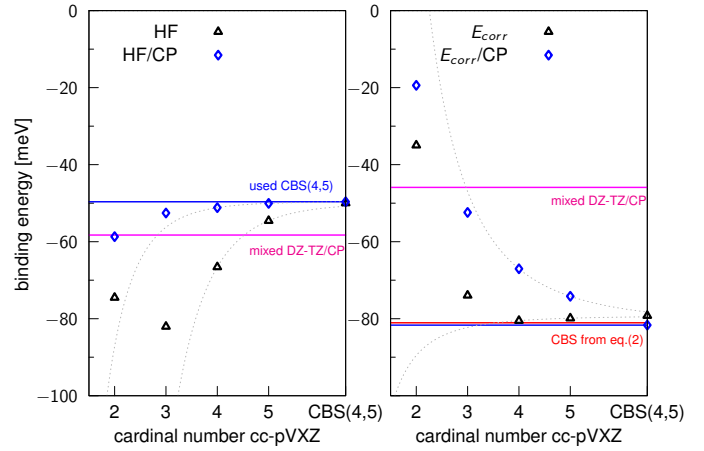


Figure 7: Binding energy separated into HF and correlation ($E_{\text{corr}}^{\text{L-CCSD(T)}}$) contributions for water adsorption on benzene in 2-leg geometry ($d_{\text{ad}} = 3.51$ Å) and increasingly large basis set expansion. Results from a mixed DZ/TZ basis set as in Ref.³⁰ and extrapolation according to eq. 6 are shown.

basis sets⁷⁹ to minimize the associated errors. The basis set artefacts on the correlation energy are more complex. Again, BSSE would lead to an overestimated binding energy, while basis set incompleteness errors typically lead to an underestimated binding energy (missing correlation effects). This can lead to uncorrected correlation energies that are closer to the basis set limit compared to the CP-corrected ones. However, this trend is not clear and the convergence is much smoother using the CP-corrected energies (see Fig. 7), which makes the extrapolation more reliable. In our study, the CCSD(T) correlation energies are extrapolated using the largest basis set results from L-CCSD(T) and extrapolating it with RPA correlation energies in the multiplicative scheme

$$E_{\text{corr}}[\text{CC/CSB}] = E_{\text{corr}}(\text{CC/QZ}) \times \frac{E_{\text{corr}}(\text{RPA/CBS})}{E_{\text{corr}}(\text{RPA/QZ})} \quad (6)$$

The CP corrected energies are reported as final results; the non-CP corrected ones give an indication of the basis set completeness. The extrapolation scheme has been chosen to minimize this error estimate (compared to e.g. the additive scheme). For benzene adsorption, we compared this to direct cc-pV(QZ,5Z) extrapolations and deviations in binding energies are below 1 meV (see Fig. 7). In contrast, a previously used combination of DZ and TZ basis sets (setting identical to Ref.³⁰) have errors of about 30 meV for the correlation energy. This partially cancels with errors on the HF energy, however, due to the functionally different convergence of HF and E_{corr} we shouldn't expect this cancellation to be consistent for different system sizes. Errors in our L-CCSD(T) energies due to pair-thresholds and non-canonical triples (T0) are estimated for benzene ad-

sorption by comparison to conventional CCSD(T) in cc-pVTZ basis to be below 5 meV, which is comparable to previous tests.^{54,87} Overall, the errors introduced by the truncation, the non-canonical triples, and the basis set extrapolation seem to be under control and below 10 meV.

Periodic CCSD(T) calculations have been carried out following the strategy outlined in Ref.⁴⁴ employing a slightly smaller 4×4 graphene cell. Periodic HF orbitals have been computed in a PAW basis with an kinetic energy cutoff for the plane wave basis of 500 eV, whereas virtual orbitals in the CCSD calculations are projected to a pseudized aug-cc-pVTZ basis set, in a PAW representation.⁸⁸ Perturbative triples (T) are evaluated using the smaller cc-pVDZ basis set to represent the virtual orbitals. The CP corrected interaction energy is defined as

$$E_{\text{int}} = E_{\text{H}_2\text{O}+\text{Graphene}} - E_{\text{H}_2\text{O}} - E_{\text{Graphene}}. \quad (7)$$

Finite-size corrections have been computed at the CCSD level⁸⁹ (-17, -16 and -19 meV for the 0-,1- and 2-leg structure, respectively). Finite coverage effects are corrected for at the HF level only using a 5×5 graphene cell (-2, 1 and 2 meV for the 0-,1- and 2-leg structure, respectively). Corrections to the vacuum size are computed using a supercell with a 30 Å vacuum distance at the MP2 level (6, 8 and 7 meV for the 0-,1- and 2-leg structure, respectively). A basis set correction is also included and is defined as the difference between the full plane-wave basis set calculation and the aug-cc-pVTZ one at the MP2 level (-4, -5 and -5 meV for the 0-,1- and 2-leg structure, respectively).

Quantum Monte Carlo

DMC calculations were performed with the CASINO code.³⁷ The adsorption energy E_{ad} is calculated as prescribed in Eq. 1, with $d_{\text{far}} \sim 10$ Å. This evaluation is more efficient than the use of the separate fragments in place of the far away configuration, as it reduces the time step bias.³⁵ However, the system at $d_{\text{far}} \sim 10$ Å could have a little residual interaction energy, which was evaluated via L-CCSD(T) to be 2.2 meV for the water-benzene system and 5.5 meV for the water-coronene system. Thus, the DMC evaluations were corrected for this interaction energy, in order to facilitate the comparison with the binding energies obtained via L-CCSD(T) and RPA, which took as reference the energy of the isolated fragments. For the graphene adsorption this residual interaction diminishes well below 1 meV as estimated by DFT calculations (PBE-D3 and PBE-MBD). Similar to Refs.,^{22,90} we used Dirac-Fock pseudopotentials^{91,92} with the locality approximation.⁹³ Single particle wave functions were obtained using DFT with the LDA functional and a plane-wave cutoff of 600 Ry, re-expanded in terms of B-splines⁹⁴ with the natural grid spacing $a = \pi/G_{\text{max}}$, where G_{max} is the magnitude of the largest plane wave in the expansion. The Jastrow factor used

in the trial wavefunction of the system included a two-body electron-electron (e-e) term; two-body electron-nucleus (e-n) terms and three-body electron-electron-nucleus (e-e-n) terms specific for any atom type. The variational parameters of the Jastrow have been optimized in order to minimize the variational variance. The time step dependence has been investigated explicitly considering values of τ ranging from 10^{-1} au to 10^{-3} au for a subset of configurations, as reported in the *Supporting Information*. Production calculations for water-benzene and water-coronene systems used a time step of 0.01 au, and in water-graphene we used $\tau = 0.025$ au. These values give a bias smaller than the stochastic error. DMC calculations were performed with a population of tens of thousands of walkers or more. We tested the population bias, which appears to be negligible with respect to the stochastic error in the production calculations (the population bias becomes of the order of a few meV only for a population of a few hundred walkers) as shown in the *Supporting Information*. In this work we are evaluating the interaction energy as the difference of two configurations both affected by FSE, thus we will benefit from a large FSE cancellation, as observed in other systems.^{54,68} Similar to Ref.,⁶⁸ we have estimated the residual FSE correction using the approach of Kwee, Zhang and Krakauer.⁹⁵ (KZK). In a subset of the configurations we checked the reliability of KZK against the more accurate (and computationally more expensive) model periodic Coulomb (MPC) approach.⁹⁶⁻⁹⁸ The estimated FSE correction on DMC binding values are reported in Fig. 8.

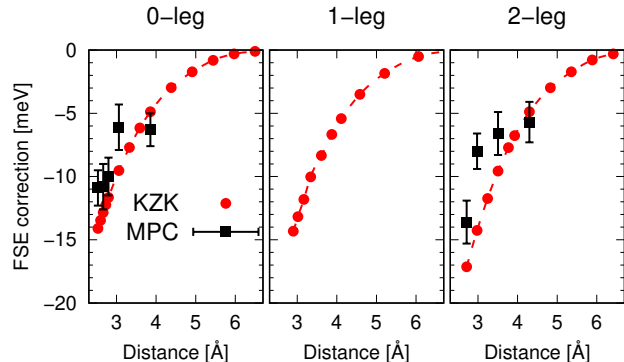


Figure 8: FSE correction in DMC for the interaction energy of water on graphene, as obtained using KZK⁹⁵ and MPC⁹⁶⁻⁹⁸ approaches, shown as a function of the distance between the oxygen of water and the graphene sheet.

References

- (1) Fumagalli, L.; Esfandiari, A.; Fabregas, R.; Hu, S.; Ares, P.; Janardanan, A.; Yang, Q.; Radha, B.; Taniguchi, T.; Watanabe, K. et al. Anomalously

- low dielectric constant of confined water. *Science (New York, NY)* **2018**, *360*, 1339–1342.
- (2) Abraham, J.; Vasu, K. S.; Williams, C. D.; Gopinadhan, K.; Su, Y.; Cherian, C. T.; Dix, J.; Prestat, E.; Haigh, S. J.; Grigorieva, I. V. et al. Tunable sieving of ions using graphene oxide membranes. *Nature Nanotechnology* **2017**, *12*, 546–550.
 - (3) Joshi, R. K.; Carbone, P.; Wang, F. C.; Kravets, V. G.; Su, Y.; Grigorieva, I. V.; Wu, H. A.; Geim, A. K.; Nair, R. R. Precise and Ultrafast Molecular Sieving Through Graphene Oxide Membranes. *Science* **2014**, *343*, 752–754.
 - (4) Nair, R. R.; Wu, H. A.; Jayaram, P. N.; Grigorieva, I. V.; Geim, A. K. Unimpeded permeation of water through helium leak tight graphene based membranes. *Science* **2012**, *335*, 442–445.
 - (5) Algara-Siller, G.; Lehtinen, O.; Wang, F. C.; Nair, R. R.; Kaiser, U.; Wu, H. A.; Geim, A. K.; Grigorieva, I. V. Square ice in graphene nanocapillaries. *Nature* **2015**, *519*, 443–445.
 - (6) Secchi, E.; Marbach, S.; Niguès, A.; Stein, D.; Siria, A.; Bocquet, L. Massive radius-dependent flow slippage in carbon nanotubes. *Nature* **2016**, *537*, 210–213.
 - (7) Radha, B.; Esfandiar, A.; Wang, F. C.; Rooney, A. P.; Gopinadhan, K.; Keerthi, A.; Mishchenko, A.; Janardanan, A.; Blake, P.; Fumagalli, L. et al. Molecular transport through capillaries made with atomic-scale precision. *Nature* **2016**, *538*, 222.
 - (8) Siria, A.; Bocquet, M.-L.; Bocquet, L. New avenues for the large-scale harvesting of blue energy. *Nature Reviews Chemistry* **2017**, *1*, 0091.
 - (9) Yoshida, H.; Kaiser, V.; Rotenberg, B.; Bocquet, L. Driplons as localized and superfast ripples of water confined between graphene sheets. *Nature Communications* **2018**, *9*, 1496.
 - (10) Hummer, G.; Rasaiah, J. C.; Noworyta, J. P. Water conduction through the hydrophobic channel of a carbon nanotube. *Nature* **2001**, *414*, 188–190.
 - (11) Strogatz, S. H.; Abrams, D. M.; McRobie, A.; Eckhardt, B.; Ott, E. Theoretical mechanics: Crowd synchrony on the Millennium Bridge. *Nature* **2005**, *438*, 43–44.
 - (12) Holt, J. K. Fast Mass Transport Through Sub-2-Nanometer Carbon Nanotubes. *Science (New York, NY)* **2006**, *312*, 1034–1037.
 - (13) Tocci, G.; Joly, L.; Michaelides, A. Friction of Water on Graphene and Hexagonal Boron Nitride from Ab Initio Methods: Very Different Slippage Despite Very Similar Interface Structures. *Nano Lett.* **2014**, *14*, 6872–6877.
 - (14) Michaelides, A. Slippery when narrow. *Nature* **2016**, *537*, 171–172.
 - (15) Esfandiar, A.; Radha, B.; Wang, F. C.; Yang, Q.; Hu, S.; Garaj, S.; Nair, R. R.; Geim, A. K.; Gopinadhan, K. Size effect in ion transport through angstrom-scale slits. *Science (New York, NY)* **2017**, *358*, 511–513.
 - (16) Li, J.; Wang, F. Water graphene contact surface investigated by pairwise potentials from force-matching PAW-PBE with dispersion correction. *J. Chem. Phys.* **2017**, *146*, 054702.
 - (17) Andrews, J. E.; Sinha, S.; Chung, P. W.; Das, S. Wetting dynamics of a water nanodrop on graphene. *Phys. Chem. Chem. Phys.* **2016**, *18*, 23482–23493.
 - (18) Yiapanis, G.; Makarucha, A. J.; Baldauf, J. S.; Downton, M. T. Simulations of graphitic nanoparticles at air-water interfaces. *Nanoscale* **2016**, *8*, 19620–19628.
 - (19) Li, Z.; Wang, Y.; Kozbial, A.; Shenoy, G.; Zhou, F.; McGinley, R.; Ireland, P.; Morganstein, B.; Kunkel, A.; Surwade, S. P. et al. Effect of airborne contaminants on the wettability of supported graphene and graphite. *Nat. Mater.* **2013**, *12*, 925.
 - (20) Prydatko, A. V.; Belyaeva, L. A.; Jiang, L.; Lima, L. M. C.; Schneider, G. F. Contact angle measurement of free-standing square-millimeter single-layer graphene. *Nat. Mater.* **2018**, *9*, 4185.
 - (21) Björneholm, O.; Hansen, M. H.; Hodgson, A.; Liu, L.-M.; Limmer, D. T.; Michaelides, A.; Pedevilla, P.; Rossmeisl, J.; Shen, H.; Tocci, G. et al. Water at Interfaces. *Chem. Rev.* **2016**, *116*, 7698–7726.
 - (22) Ma, J.; Michaelides, A.; Alfè, D.; Schimka, L.; Kresse, G.; Wang, E. Adsorption and diffusion of water on graphene from first principles. *Phys. Rev. B* **2011**, *84*, 033402.
 - (23) Hamada, I. Adsorption of water on graphene: A van der Waals density functional study. *Phys. Rev. B* **2012**, *86*, 195436.
 - (24) Silvestrelli, P. L.; Ambrosetti, A. Including screening in van der Waals corrected density functional theory calculations: The case of atoms and small molecules physisorbed on graphene. *J. Chem. Phys.* **2014**, *140*, 124107.

- (25) Lorenz, M.; Civalleri, B.; Maschio, L.; Sgroi, M.; Pullini, D. Benchmarking dispersion and geometrical counterpoise corrections for cost-effective large-scale DFT calculations of water adsorption on graphene. *J. Comput. Chem.* **35**, 1789–1800.
- (26) Leenaerts, O.; Partoens, B.; Peeters, F. M. Water on graphene: Hydrophobicity and dipole moment using density functional theory. *Phys. Rev. B* **2009**, *79*, 235440.
- (27) Heßelmann, A. Assessment of a Nonlocal Correction Scheme to Semilocal Density Functional Theory Methods. *J. Chem. Theory Comput.* **2013**, *9*, 273–283.
- (28) Rubeš, M.; Nachtigall, P.; Vondrášek, J.; Bludský, O. Structure and Stability of the Water-Graphite Complexes. *J. Phys. Chem. C* **2009**, *113*, 8412–8419.
- (29) Jenness, G. R.; Karalti, O.; Jordan, K. D. Benchmark calculations of water-acene interaction energies: Extrapolation to the water-graphene limit and assessment of dispersion-corrected DFT methods. *Phys. Chem. Chem. Phys.* **2010**, *12*, 6375–6381.
- (30) Voloshina, E.; Usvyat, D.; Schutz, M.; Dedkov, Y.; Paulus, B. On the physisorption of water on graphene: a CCSD(T) study. *Phys. Chem. Chem. Phys.* **2011**, *13*, 12041–12047.
- (31) Michaelides, A.; Martinez, T. J.; Alavi, A.; Kresse, G.; Manby, F. R. Preface: Special Topic Section on Advanced Electronic Structure Methods for Solids and Surfaces. *J. Chem. Phys.* **2015**, *143*, 102601.
- (32) Feller, D.; Jordan, K. D. Estimating the Strength of the Water/Single-Layer Graphite Interaction. *J. Phys. Chem. A* **2000**, *104*, 9971–9975.
- (33) Ideally, the energy for non-interacting systems $E_{W+G}(d_{\text{far}})$ should be evaluated at a distance $d_{\text{far}} \rightarrow \infty$. Computationally, there are two alternative ways to calculate $E_{W+G}(d_{\text{far}})$: *i.* consider a finite value of d_{far} that makes the residual interaction energy negligible with respect to the needed accuracy; *ii.* evaluate as the summation of the energy of the water and graphene fragments. The two methods are in principle equivalent for size-consistent electronic structure approaches, however in periodic systems (so, in presence of finite size errors) the former method typically benefits from a better error cancellation and allows the use of smaller simulation cells.
- (34) Foulkes, W. M. C.; Mitas, L.; Needs, R. J.; Rajagopal, G. Quantum Monte Carlo simulations of solids. *Rev. Mod. Phys.* **2001**, *73*, 33–83.
- (35) Zen, A.; Sorella, S.; Gillan, M. J.; Michaelides, A.; Alfè, D. Boosting the accuracy and speed of quantum Monte Carlo: size-consistency and time-step. *Phys. Rev. B* **2016**, *93*, 241118(R).
- (36) Zen, A.; Brandenburg, J. G.; Klimeš, J.; Tkatchenko, A.; Alfè, D.; Michaelides, A. Fast and accurate quantum Monte-Carlo for molecular crystals. *Proc. Natl. Acad. Sci. U.S.A.* **2018**, *115*, 1724–1729.
- (37) Needs, R. J.; Towler, M. D.; Drummond, N. D.; Rios, P. L. Continuum variational and diffusion quantum Monte Carlo calculations. *J. Phys.: Condens. Matter* **2010**, *22*, 023201.
- (38) Riplinger, C.; Sandhoefer, B.; Hansen, A.; Neese, F. Natural Triple Excitations in Local Coupled Cluster Calculations with Pair Natural Orbitals. *J. Chem. Phys.* **2013**, *139*, 134101.
- (39) Neese, F. The ORCA program system. *WIREs Comput. Mol. Sci.* **2012**, *2*, 73–78.
- (40) Booth, G. H.; Grüneis, A.; Kresse, G.; Alavi, A. Towards an exact description of electronic wavefunctions in real solids. *Nature* **2013**, *493*, 365.
- (41) Kresse, G.; Furthmüller, J. Efficiency of ab-initio total energy calculations for metals and semiconductors using a plane-wave basis set. *J. Comp. Mat. Sci.* **1996**, *6*, 15.
- (42) Kresse, G.; Furthmüller, J. Efficient iterative schemes for ab initio total-energy calculations using a plane-wave basis set. *Phys. Rev. B* **1996**, *54*, 11169.
- (43) Hummel, F.; Tsatsoulis, T.; Grüneis, A. Low rank factorization of the Coulomb integrals for periodic coupled cluster theory. *J. Chem. Phys.* **2017**, *146*, 124105.
- (44) Gruber, T.; Liao, K.; Tsatsoulis, T.; Hummel, F.; Grüneis, A. Applying the Coupled-Cluster Ansatz to Solids and Surfaces in the Thermodynamic Limit. *Phys. Rev. X* **2018**, *8*, 021043.
- (45) Nozières, P.; Pines, D. Correlation Energy of a Free Electron Gas. *Phys. Rev.* **1958**, *111*, 442–454.
- (46) Harl, J.; Kresse, G. Cohesive energy curves for noble gas solids calculated by adiabatic connection fluctuation-dissipation theory. *Phys. Rev. B* **2008**, *77*, 045136.
- (47) Harl, J.; Kresse, G. Accurate Bulk Properties from Approximate Many-Body Techniques. *Phys. Rev. Lett.* **2009**, *103*, 056401.

- (48) Eshuis, H.; Bates, J. E.; Furche, F. Electron correlation methods based on the random phase approximation. *Theo. Chem. Acc.* **2012**, *131*, 1084.
- (49) Wilhelm, J.; Seewald, P.; Del Ben, M.; Hutter, J. Large-Scale Cubic-Scaling Random Phase Approximation Correlation Energy Calculations Using a Gaussian Basis. *J. Chem. Theory Comput.* **2016**, *12*, 5851–5859.
- (50) Schimka, L.; Harl, J.; Stroppa, A.; Grüneis, A.; Marsman, M.; Mittendorfer, F.; Kresse, G. Accurate surface and adsorption energies from many-body perturbation theory. *Nat. Mater.* **2010**, *9*, 741–744.
- (51) Ren, X.; Tkatchenko, A.; Rinke, P.; Scheffler, M. Beyond the Random-Phase Approximation for the Electron Correlation Energy: The Importance of Single Excitations. *Phys. Rev. Lett.* **2011**, *106*, 153003.
- (52) Klimeš, J. Lattice energies of molecular solids from the random phase approximation with singles corrections. *J. Chem. Phys.* **2016**, *145*, 094506.
- (53) Klimeš, J.; Kaltak, M.; Maggio, E.; Kresse, G. Singles correlation energy contributions in solids. *J. Chem. Phys.* **2015**, *143*, 102816.
- (54) Al-Hamdani, Y. S.; Rossi, M.; Alfè, D.; Tsatsoulis, T.; Ramberger, B.; Brandenburg, J. G.; Zen, A.; Kresse, G.; Grüneis, A.; Tkatchenko, A. et al. Properties of the water to boron nitride interaction: From zero to two dimensions with benchmark accuracy. *J. Chem. Phys.* **2017**, *147*, 044710.
- (55) We define the substrate size as the circle in the substrate plane with minimal radius, where all atom positions are within the circle (see inset of Fig. 4).
- (56) Note that this trend is still possible within the stochastic error of the DMC data.
- (57) Kim, H.-Y.; dos Santos, M. C.; Cole, M. W. Wetting Transitions of Water on Graphite and Graphene. *J. Phys. Chem. A* **2014**, *118*, 8237–8241.
- (58) McKenzie, S.; Kang, H. C. Squeezing water clusters between graphene sheets: energetics, structure, and intermolecular interactions. *Phys. Chem. Chem. Phys.* **2014**, *16*, 26004–26015.
- (59) Ma, M.; Tocci, G.; Michaelides, A.; Aeppli, G. Fast diffusion of water nanodroplets on graphene. *Nature Materials* **2015**, *15*, 66.
- (60) Wu, Y.; Aluru, N. R. Graphitic Carbon-Water Nonbonded Interaction Parameters. *J. Phys. Chem. B* **2013**, *117*, 8802–8813.
- (61) Werder, T.; Walther, J. H.; Jaffe, R. L.; Halicioglu, T.; Koumoutsakos, P. On the Water-Carbon Interaction for Use in Molecular Dynamics Simulations of Graphite and Carbon Nanotubes. *J. Phys. Chem. B* **2003**, *107*, 1345–1352.
- (62) Leroy, F.; Liu, S.; Zhang, J. Parametrizing Non-bonded Interactions from Wetting Experiments via the Work of Adhesion: Example of Water on Graphene Surfaces. *J. Phys. Chem. C* **2015**, *119*, 28470–28481.
- (63) Hohenstein, E. G.; Sherrill, C. D. Density fitting and Cholesky decomposition approximations in symmetry-adapted perturbation theory: Implementation and application to probe the nature of π - π interactions in linear acenes. *J. Chem. Phys.* **2010**, *132*, 184111.
- (64) Heßelmann, A.; Jansen, G.; Schütz, M. Density-functional theory-symmetry-adapted intermolecular perturbation theory with density fitting: A new efficient method to study intermolecular interaction energies. *J. Chem. Phys.* **2005**, *122*, 014103.
- (65) Jansen, G. Symmetry-Adapted Perturbation Theory Based on Density Functional Theory for Non-covalent Interactions. *WIREs Comput. Mol. Sci.* **2014**, *4*, 127–144.
- (66) Szalewicz, K. Symmetryadapted perturbation theory of intermolecular forces. *WIREs Comput. Mol. Sci.* **2012**, *2*, 254–272.
- (67) Al-Hamdani, Y. S.; Alfè, D.; Michaelides, A. How strongly do hydrogen and water molecules stick to carbon nanomaterials? *J. Chem. Phys.* **2017**, *146*, 094701.
- (68) Zen, A.; Roch, L. M.; Cox, S. J.; Hu, X. L.; Sorella, S.; Alfè, D.; Michaelides, A. Toward Accurate Adsorption Energetics on Clay Surfaces. *J. Phys. Chem. C* **2016**, *120*, 26402–26413.
- (69) Binnie, S. J.; Nolan, S. J.; Drummond, N. D.; Alfè, D.; Allan, N. L.; Manby, F. R.; Gillan, M. J. Bulk and surface energetics of crystalline lithium hydride: Benchmarks from quantum Monte Carlo and quantum chemistry. *Phys. Rev. B* **2010**, *82*, 165431.
- (70) Tsatsoulis, T.; Hummel, F.; Usvyat, D.; Schütz, M.; Booth, G. H.; Binnie, S. S.; Gillan, M. J.; Alfè, D.; Michaelides, A.; Grüneis, A. A comparison between quantum chemistry and quantum Monte Carlo techniques for the adsorption of water on the (001) LiH surface. *J. Chem. Phys.* **2017**, *146*, 204108.

- (71) Perdew, J. P.; Burke, K.; Ernzerhof, M. Generalized Gradient Approximation Made Simple. *Phys. Rev. Lett.* **1996**, *77*, 3865–3868, erratum *Phys. Rev. Lett.* **78**, 1396 (1997).
- (72) Grimme, S.; Antony, J.; Ehrlich, S.; Krieg, H. A consistent and accurate ab initio parametrization of density functional dispersion correction (DFT-D) for the 94 elements H-Pu. *J. Chem. Phys.* **2010**, *132*, 154104.
- (73) Grimme, S.; Hansen, A.; Brandenburg, J. G.; Banwarth, C. Dispersion-Corrected Mean-Field Electronic Structure Methods. *Chem. Rev.* **2016**, *116*, 5105–5154.
- (74) Molinero, V.; Moore, E. B. Water Modeled As an Intermediate Element between Carbon and Silicon. *J. Phys. Chem. B* **2009**, *113*, 4008–4016.
- (75) Plimpton, S. Fast Parallel Algorithms for Short-Range Molecular Dynamics. *J. Comput. Phys.* **1995**, *117*, 1–19.
- (76) Martyna, G. J.; Klein, M. L.; Tuckerman, M. Nosé-Hoover chains: The canonical ensemble via continuous dynamics. *J. Chem. Phys.* **1992**, *97*, 2635–2643.
- (77) Boruvka, L.; Neumann, A. Generalization of the classical theory of capillarity. *J. Chem. Phys.* **1977**, *66*, 5464–5476.
- (78) Furche, F.; Ahlrichs, R.; Hättig, C.; Klopper, W.; Sierka, M.; Weigend, F. Turbomole. *WIREs Comput Mol Sci* **2014**, *4*, 91–100.
- (79) Neese, F.; Hansen, A.; Liakos, D. G. Efficient and accurate approximations to the local coupled cluster singles doubles method using a truncated pair natural orbital basis. *J. Chem. Phys.* **2009**, *131*, 064103.
- (80) Kaltak, M.; Klimeš, J.; Kresse, G. Low scaling algorithms for the random phase approximation: Imaginary time and Laplace transformations. *J. Chem. Theo. Comput.* **2014**, *10*, 2498.
- (81) Kaltak, M.; Klimeš, J.; Kresse, G. Cubic scaling algorithm for the random phase approximation: Self-interstitials and vacancies in Si. *Phys. Rev. B* **2014**, *90*, 054115.
- (82) Riplinger, C.; Pinski, P.; Becker, U.; Valeev, E. F.; Neese, F. Sparse maps – A systematic infrastructure for reduced-scaling electronic structure methods. II. Linear scaling domain based pair natural orbital coupled cluster theory. *J. Chem. Phys.* **2016**, *144*, 024109.
- (83) Halkier, A.; Helgaker, T.; Jørgensen, P.; Klopper, W.; Koch, H.; Olsen, J.; Wilson, A. K. Basis-set convergence in correlated calculations on Ne, N₂, and H₂O. *Chem. Phys. Lett.* **1998**, *286*, 243 – 252.
- (84) Truhlar, D. G. Basis-set extrapolation. *Chem. Phys. Lett.* **1998**, *294*, 45 – 48.
- (85) Jurečka, P.; Šponer, J.; Cerny, J.; Hobza, P. Benchmark Database of Accurate (MP2 and CCSD(T) Complete Basis Set Limit) Interaction Energies of Small Model Complexes, DNA Base Pairs, and Amino Acid Pairs. *Phys. Chem. Chem. Phys.* **2006**, *8*, 1985–1993.
- (86) Kruse, H.; Mladek, A.; Gkionis, K.; Hansen, A.; Grimme, S.; Sponer, J. Quantum Chemical Benchmark Study on 46 RNA Backbone Families Using a Dinucleotide Unit. *J. Chem. Theory Comput.* **2015**, *11*, 4972–4991.
- (87) Guo, Y.; Riplinger, C.; Becker, U.; Liakos, D. G.; Minenkov, Y.; Cavallo, L.; Neese, F. Communication: An improved linear scaling perturbative triples correction for the domain based local pair-natural orbital based singles and doubles coupled cluster method [DLPNO-CCSD(T)]. *J. Chem. Phys.* **2018**, *148*, 011101.
- (88) Booth, G. H.; Tsatsoulis, T.; Chan, G. K.-L.; Grüneis, A. From plane waves to local Gaussians for the simulation of correlated periodic systems. *The Journal of Chemical Physics* **2016**, *145*.
- (89) Liao, K.; Grüneis, A. Communication: Finite size correction in periodic coupled cluster theory calculations of solids. *J. Chem. Phys.* **2016**, *145*, 141102.
- (90) Ma, J.; Alfè, D.; Michaelides, A.; Wang, E. The water-benzene interaction: Insight from electronic structure theories. *J. Chem. Phys.* **2009**, *130*, 154303.
- (91) Trail, J. R.; Needs, R. J. Norm-conserving Hartree-Fock pseudopotentials and their asymptotic behavior. *J. Chem. Phys.* **2005**, *122*, 014112.
- (92) Trail, J. R.; Needs, R. J. Smooth relativistic Hartree-Fock pseudopotentials for H to Ba and Lu to Hg. *J. Chem. Phys.* **2005**, *122*, 174109.
- (93) Mitas, L.; Shirley, E. L.; Ceperley, D. M. Nonlocal pseudopotentials and diffusion Monte Carlo. *J. Chem. Phys.* **1991**, *95*, 3467.
- (94) Alfè, D.; Gillan, M. J. Efficient localized basis set for quantum Monte Carlo calculations on condensed matter. *Phys. Rev. B* **2004**, *70*, 161101.

- (95) Kwee, H.; Zhang, S.; Krakauer, H. Finite-Size Correction in Many-Body Electronic Structure Calculations. *Phys. Rev. Lett.* **2008**, *100*, 126404.
- (96) Fraser, L. M.; Foulkes, W. M. C.; Rajagopal, G.; Needs, R. J.; Kenny, S. D.; Williamson, A. J. Finite-size effects and Coulomb interactions in quantum Monte Carlo calculations for homogeneous systems with periodic boundary conditions. *Phys. Rev. B* **1996**, *53*, 1814–1832.
- (97) Williamson, A. J.; Rajagopal, G.; Needs, R. J.; Fraser, L. M.; Foulkes, W. M. C.; Wang, Y.; Chou, M.-Y. Elimination of Coulomb finite-size effects in quantum many-body simulations. *Phys. Rev. B* **1997**, *55*, R4851–R4854.
- (98) Kent, P. R. C.; Hood, R. Q.; Williamson, A. J.; Needs, R. J.; Foulkes, W. M. C.; Rajagopal, G. Finite-size errors in quantum many-body simulations of extended systems. *Phys. Rev. B* **1999**, *59*, 1917–1929.